Available online at www.sciencedirect.com
SCIENCE DIRECT®
Journal of Molecular Catalysis A: Chemical 234 (2005) 75–83
JOURNAL OF MOLECULAR CATALYSIS A: CHEMICAL
www.elsevier.com/locate/molcata

Fe modified $CuMnZrO_2$ catalysts for higher alcohols synthesis from syngas: Effect of calcination temperature

Run Xu [a], Wei Wei [a], Wen-huai Li [a], Tian-dou Hu [b], Yu-han Sun [a,*]

[a] *State Key Laboratory of Coal Conversion, Institute of Coal Chemistry, Chinese Academy of Sciences, Taiyuan 030001, PR China*
[b] *Beijing Synchrotron Radiation Facility, Institute of High Energy Physics, Chinese Academy of Sciences, Beijing 100039, PR China*

Received 10 November 2004; received in revised form 27 January 2005; accepted 27 January 2005
Available online 7 April 2005

Abstract

The structure and catalytic performance of $CuMnZrO_2$ and Fe-$CuMnZrO_2$ catalysts, which were calcined at different temperature, were investigated by BET, XRD, N_2O-titration, XANES, EXAFS and TPR. It was found that the calcination temperature strongly influenced the interaction between the active species and support and hence the structure and catalytic performance. Low calcination temperature yielded poorly crystallized catalysts and favored the formation of a $Cu(OH)_2$-like structure. The presence of iron could suppress crystallization of amorphous zirconia and increased the dispersion of copper due to the iron–zirconia interaction within the rise of calcination temperature from 623 to 873 K. However, the addition of iron resulted in the decrease of catalytic activity and selectivity. This could be explained by strong iron–zirconia interaction. It led to the decrease of copper–zirconia interaction, which was responsible for the methanol synthesis, and the decrease of copper–iron interaction, which was responsible for the formation of higher alcohols.

Keywords: Structure; Fe-$CuMnZrO_2$; Higher alcohols; Calcination temperature

1. Introduction

The production of C_1–C_6 alcohol mixtures can be considered as a possible added value pathway for natural gas passing through the intermediacy of syngas [1]. The obtained alcohols have been proposed for various utilizations such as solvent, fuel, or additives such as octane boosters in gasoline [2]. Among the several categories of catalysts for mixed alcohols synthesis [3,4], Fischer–Tropsch elements (Fe, Co, Ni, Ru) modified copper based catalysts have drawn a widely attention because of their high activity and selectivity, such as Co-$CuZnOAl_2O_3$ [5–7], Co-CuZnCr [8] and Co-$CuLaZrO_2$ catalysts [9]. Those researches showed that the synergism was the result of interaction between cobalt and copper [10]. The cobalt was thought to provide the C–C chain growth, while copper would be responsible for chain termination [7]. Moreover, Bailliard–Letournel et al. [11] found that the interaction of copper and cobalt in Cu-Co catalysts led to a surface alloy, and proposed that such an alloy was responsible for the high selectivity to alcohols. But the metal-support interaction or cobalt alumina spinel phase formation could strongly inhibit the interaction between copper and cobalt [12], and the preparation parameters were found to have the greatly influence on the formation of copper–cobalt phase or cobalt alumina spinel phase [13].

In our earlier research, we found that the Fischer–Tropsch elements (Fe, Co, Ni) modified $CuZrO_2$ catalysts showed relatively high activity and selectivity for mixed alcohols synthesis [14]. It was thought that the Cu–M (M=Fe, Co, Ni) phases were the active sites for higher alcohol formation. The effect of iron on the adsorption properties of $CuMnZrO_2$ catalysts was investigated used TPD and FTIR spectroscopy in our previous paper [15]. It was found that the adsorption features of catalysts changed significantly with the addition of iron. The interactions that took place among the active phases or between the metal and support generally influenced

* Corresponding author. Fax: +86 351 4041153.
E-mail address: yhsun@sxicc.ac.cn (Y.-h. Sun).

1381-1169/$ – see front matter © 2005 Elsevier B.V. All rights reserved.
doi:10.1016/j.molcata.2005.01.048

the surface and structural properties of the catalyst and hence the catalytic performance. However, the catalysts system of Fe-$CuMnZrO_2$ was quite complex and made it difficult to understand the interaction between different components. In the present work, the effect of calcination temperature on $CuMnZrO_2$ and Fe-$CuMnZrO_2$ catalysts was investigated to establish the influence of iron on the structure of catalyst and to obtain the information on the interaction between different components. Catalytic performance was discussed in relation to the structures of the catalysts, which were clarified by the combination of BET, N_2O-adsorption, XRD, XANES, EXAFS and H_2-TPR.

2. Experimental

2.1. Preparation of catalysts

$CuMnZrO_2$ catalysts were prepared by co-precipitation of a solution of $Cu(NO_3)_2{\cdot}3H_2O$, $Mn(NO_3)_2$, and $ZrOCl_2{\cdot}8H_2O$ with an aqueous solution of Na_2CO_3 at 343 K and a constant pH of 10 in a well-stirred thermo-stated container. Then the precipitates were aged at 343 K for 2 h. After washed thoroughly with distilled water, the precipitates were dried at 393 K for 12 h, and then calcined at different temperatures in air for 3 h. Fe-$CuMnZrO_2$ catalysts were prepared using the same procedure as for $CuMnZrO_2$, except that $Fe(NO_3)_3{\cdot}9H_2O$ was introduced into the mixed solution. The composition of so-produced catalysts was as follows: Cu:Mn:Zr:Fe = 1:0.5:2:0.1 (molar ratio).

2.2. Characterization of catalysts

The BET surface areas of catalysts were determined by N_2 adsorption at 77 K using the Tristar 3000 chemical adsorption instrument (Micromeritics). Powder X-ray diffraction (XRD) patterns were recorded on a Rigaku D/Max diffractorments with a Cu target and Ni filter. Elemental analysis was determined by atomic absorption spectroscopy (Atomscan 16). For the $CuMnZrO_2$ catalysts and Fe modified catalysts, the Na content was in the range of 0.02–0.05%.

The copper surface area (S_{Cu}) was determined by using a nitrous oxide pulse method as described by Evans et al. [16]. The sample was placed in a quartz tube reactor and reduced in flowing hydrogen. After reduction, the gas flow was switched to argon and the temperature was lowered down to 353 K. A pulse of nitrous oxide was introduced into the argon flow by means of a calibrated sample valve. The exit gas was analyzed by mass spectrometer (QMS, Balzers OmniStar 200). The amount of surface copper was calculated from the amount of nitrogen evolved, assuming the dissociation of nitrous oxide takes place on surface copper followed the equation (average atom density: 1.49×10^{19} atoms m^{-2}):

$$N_2O(g) + 2Cu_s = N_2(g) + (Cu{-}O{-}Cu)_s \quad (1)$$

N_2O did not decompose on Fe–$MnZrO_2$ catalyst pre-reduced at 623 K, suggesting that any reduced iron species and manganese species presented not decompose N_2O at 353 K.

X-ray adsorption spectra (XAFS) around the Cu K-adsorption edge were obtained using the beamline of 1W1B of Beijing Synchrotron Radiation Facility (BSRF). The storage ring was operated at 2.5 GeV with a typical current of 40–60 mA. The fixed-exit Si(1 1 1) flat double crystals were used as monochromator. A sampling step of 0.5 eV for the XANES part of the spectra and a variable sampling step for EXAFS part were adopted. Spectra were collected at room temperature. EXAFS data were processed using the program for EXAFS data analysis written by the Institute of Physics, Chinese Academy of Sciences.

Temperature program reduction (TPR) was carried out in a U-tube quartz reactor. The samples (50 mg) were flushed with an argon flow of 50 cm^3 min^{-1} at 393 K to remove water and then reduced in a flow of hydrogen–argon mixture (containing 5 vol.% of hydrogen) at a rate of 10 K min^{-1} with a programmable temperature controller. Hydrogen consumption was monitored by a thermal conductivity cell (TCD) attached to a gas chromatograph (GC-950). The effluent gas was passed through a cold trap placed before TCD in order to remove water from the exit stream of the reactor.

2.3. Activity measurements

The activity tests were conducted with a fixed-bed, stainless flow micro reactor. All catalysts were reduced in a hydrogen–nitrogen mixture (containing 5 vol.% of hydrogen) flow at 573 K and atmospheric pressure before exposure to syngas. The steady-state activity measurements were taken after at least 48 h on the stream. The analysis of the gaseous and liquid products was made by Shimazu-8A gas chromatographs. H_2, CO, CH_4 and CO_2 were determined by thermal conductivity detector (TCD) equipped with a TDX-101 column. The water and methanol in liquids were also detected by TCD with a GDX-401 column. The alcohols and hydrocarbons were analyzed by flame ionization detector (FID) with a Porapak-Q column.

3. Results and discussion

3.1. Textural and structural properties of catalysts

The BET surface area of $CuMnZrO_2$ catalysts decreased continuously with the rise of calcination temperature, while the pore volume decreased and the average pore size increased (see Table 1). Particularly, when the calcination temperature was increased from 873 to 1073 K, the surface area decreased sharply from 82 to 9 m^2 g^{-1}. At the same time, the pore size increased from 11.2 to 30.4 nm. This was due to that metallic oxide particles shrink and agglomeration when they were calcined at high temperature. Compared with

Table 1
The texture parameters of Fe-$CuMnZrO_2$ catalysts calcined at different temperatures

Catalysts	Calcination temperature (K)	S_{BET} ($m^2\ g^{-1}$)	r_P (nm)	V_P ($mL\ g^{-1}$)
$CuMnZrO_2$	623	193	3.3	0.16
	723	146	6.7	0.12
	873	82	11.2	0.10
	1073	9	30.4	0.05
Fe-$CuMnZrO_2$	623	197	4.0	0.20
	723	171	4.6	0.19
	873	116	5.5	0.16
	1073	7	32.6	0.06

$CuMnZrO_2$, the presence of iron could inhibit the metallic oxide particles agglomeration. The surface area of Fe-$CuMnZrO_2$ catalyst was 171 $m^2\ g^{-1}$ at 723 K and 116 $m^2\ g^{-1}$ at 873 K, which were higher than the unprompted catalyst.

The copper dispersion measured by N_2O decomposition on catalysts was shown in Fig. 1. For the $CuMnZrO_2$, the copper dispersion was 5.7% when calcined at 623 K and decreased monotonously with the rise of calcination temperature. The presence of iron favored the formation of small copper metal crystallites on supports. The copper dispersion of Fe-$CuMnZrO_2$ calcined at 623 K was 6.6%. Moreover, the copper dispersion of Fe-$CuMnZrO_2$ slightly increased with the rise of calcination temperature from 623 to 873 K. This indicated that iron could increase the interaction between copper species and supports, which favored the dispersion of copper species. As Huang et al. [17] revealed, the re-dispersion of copper species took place during the process of calcination because of the interaction between copper species and supports. But such an improvement was limited, the copper species aggregated seriously when the catalyst was calcined above 1073 K, which led to a drastic decrease in the copper dispersion.

The X-ray diffraction pattern of $CuMnZrO_2$ catalysts did not show any peaks when the catalysts were calcined below

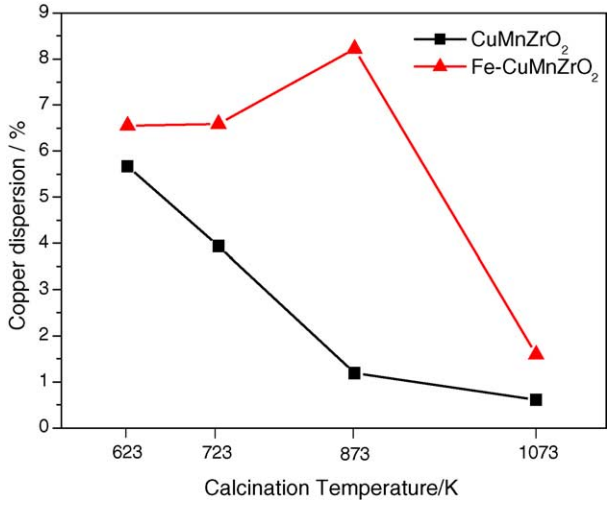

Fig. 1. The copper dispersion of catalysts calcined at various temperatures.

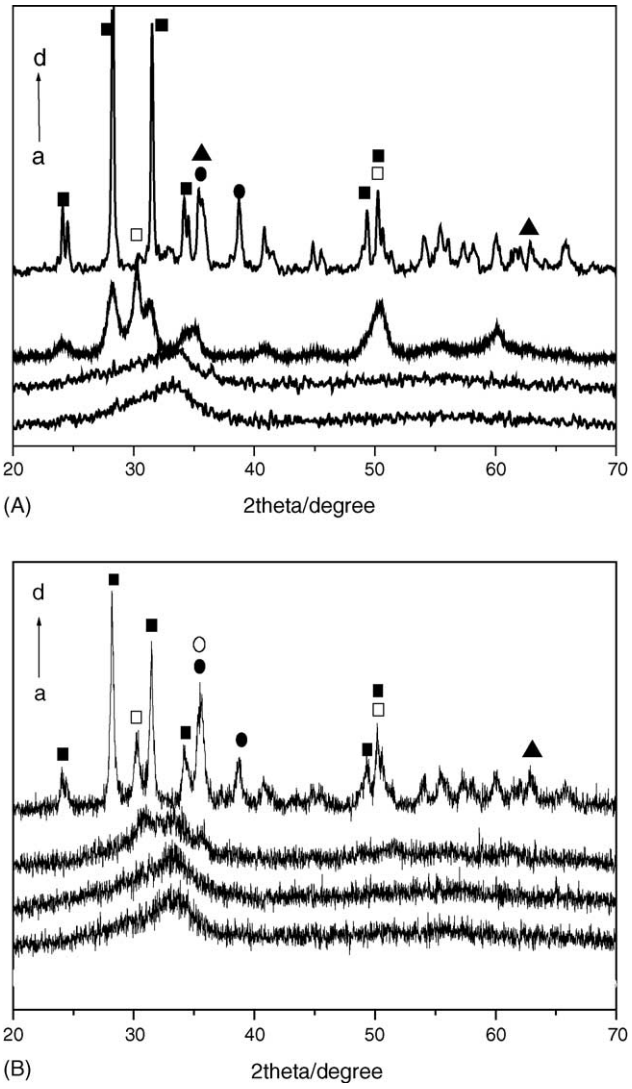

Fig. 2. XRD patters of $CuMnZrO_2$ (A) and Fe-$CuMnZrO_2$ (B) catalysts calcined at different temperatures: (a) 623 K; (b) 723 K; (c) 873 K; and (d) 1073 K. (□) t-ZrO_2; (■) m-ZrO_2; (●) CuO; (◯) $CuFe_2O_4$; and (▲) $CuMn_2O_4$.

723 K, indicating that the active phase could be well dispersed on amorphous zirconia (see Fig. 2A). The crystallite sizes were not enough large to be detected by X-ray. For the catalyst calcined at 873 K, the peaks at $2\theta = 30.2^\circ$ corresponding to the diffraction of tetragonal zirconia (t-ZrO_2), and the peaks at $2\theta = 28.3^\circ$ and 31.3° corresponding to the diffraction of monoclinic zirconia (m-ZrO_2) were observed. Moreover, the $CuMnZrO_2$ catalysts became much well crystallized at 1073 K. The diffraction peaks of m-ZrO_2 were predominant and the peaks of t-ZrO_2 became very weak. CuO exhibited major peaks at $2\theta = 38.7^\circ$ and 35.5°, while $CuMn_2O_4$ showed a peak at $2\theta = 63.2^\circ$. This indicated that the zirconia was mainly in monoclinic phase and the active species aggregated seriously at that calcination temperature.

The presence of iron greatly influenced the crystallinity of Fe-$CuMnZrO_2$ catalysts. Compared with $CuMnZrO_2$, the

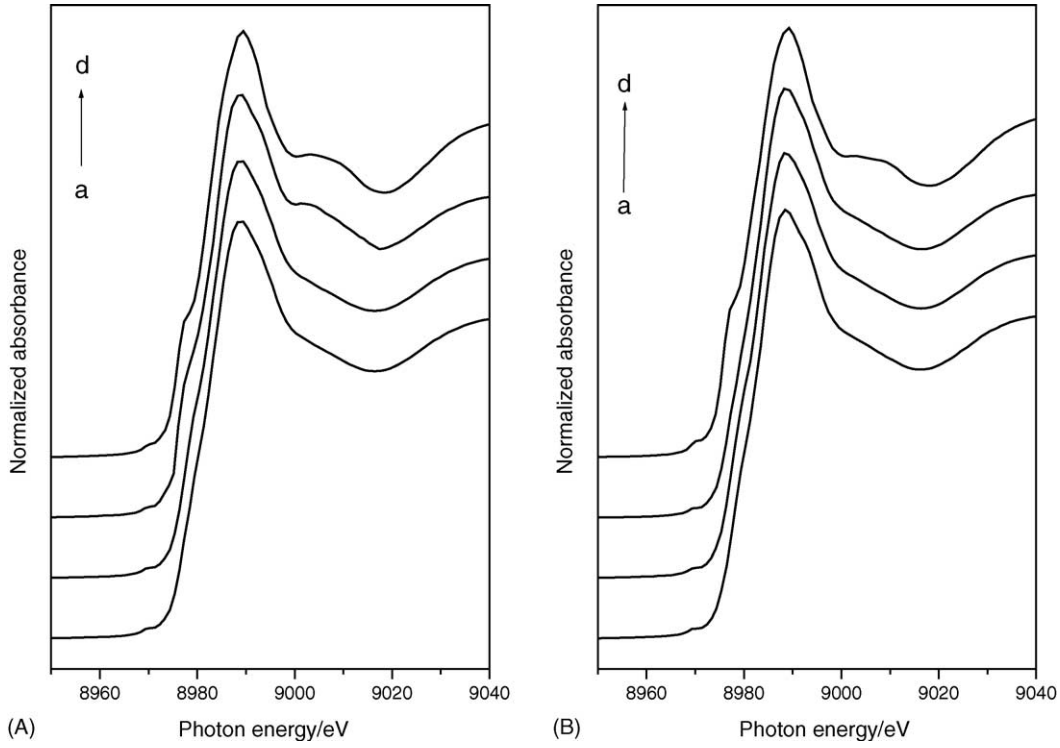

Fig. 3. Cu K-edge XANES spectra for $CuMnZrO_2$ (A) and Fe-$CuMnZrO_2$ (B) catalysts calcined at different temperature: (a) 623 K; (b) 723 K; (c) 873 K; and (d) 1073 K.

Fe-$CuMnZrO_2$ catalysts exhibited an amorphous-like or less well-ordered structure feature even if the calcination temperature was 873 K (see Fig. 2B). This suggested that the presence of iron suppressed the crystallization of zirconia. After the catalyst was calcined at 1073 K, several sharp peaks appeared. Different from $CuMnZrO_2$ catalyst, the diffraction peaks of t-ZrO_2 were still strong, indicating that the t-ZrO_2 phase was still a big fraction in the zirconia. This meant that the presence of iron could inhibit the crystal phase transformation of zirconia. Moreover, it was noteworthy that the $CuFe_2O_4$ phase exhibited a major peak at $2\theta = 35.6^\circ$. This result demonstrated that the interaction between iron and copper increased by formation of spinel compound.

3.2. XANES and EXAFS of catalysts

The XANES of the Cu K-edge of Cu catalysts have been measured to reveal the structure and electronic state of the Cu species [18–22]. Fig. 3 shows Cu K-edge XANES spectra of $CuMnZrO_2$ and iron-modified catalysts. The XANES spectra of reference compounds, CuO (Cu^{2+} in a square planar symmetry) and $Cu(OH)_2$ (Cu^{2+} in an octahedral symmetry) were shown in Fig. 4 for the comparison. The $CuMnZrO_2$ catalysts calcined at 623 and 723 K showed very close XANES spectra to that for $Cu(OH)_2$, indicating that the major Cu^{2+} species in the catalysts were in an octahedral symmetry, surrounded by six O^{2-} anions (see Fig. 3A). The presence of a weak $1s \rightarrow 3d$ pre-peak at 8977 eV supported the conclusion [23,24]. On the other hand, clear humps appeared at 8986 and 9013 eV on $CuMnZrO_2$ catalyst calcined at 873 K and their intensity increased with the rise of calcination temperature. Since CuO showed similar characteristic peaks in the XANES spectrum as presented in Fig. 4, it suggested that CuO clusters would produce at the temperature higher than 873 K.

Generally, the CuO species (Cu^{2+} in a square planar symmetry) would produce in supported Cu catalysts after calcination in air, such as Cu/α-Al_2O_3, Cu/SiO_2 and Cu/TiO_2, because CuO was more stable than $Cu(OH)_2$. But in the present study, a structure of $Cu(OH)_2$ was observed. In Cheah et al. [25] research on the Cu/amorphous SiO_2 catalysts, they also found that $Cu(OH)_2$ produced on the amorphous SiO_2 surface. A possible explanation was that the surface energy of CuO was larger than that of $Cu(OH)_2$. Consequently, $Cu(OH)_2$ would become the more stable phase when the precipitating particle sizes were small enough that surface energy was an important contribution to the free energy [26]. On the other hand, Okamoto et al. [27] investigated calcined $CuZrO_2$ catalysts using XANES and FTIR, suggesting that the highly dispersed copper species were formed by the reaction of copper oxides with the hydroxy groups on zirconia, moreover, $Cu(OH)_2$ species was detected in the catalyst. In present study, the amorphous zirconia support had abundant surface hydroxyl as many papers had reported [28]. Therefore, the highly-dispersed copper species could have a strong interaction with these surface hydroxy groups and favor the formation of $Cu(OH)_2$. When the amorphous phase transformed to t-ZrO_2 or m-ZrO_2 at higher calcination temperature, the

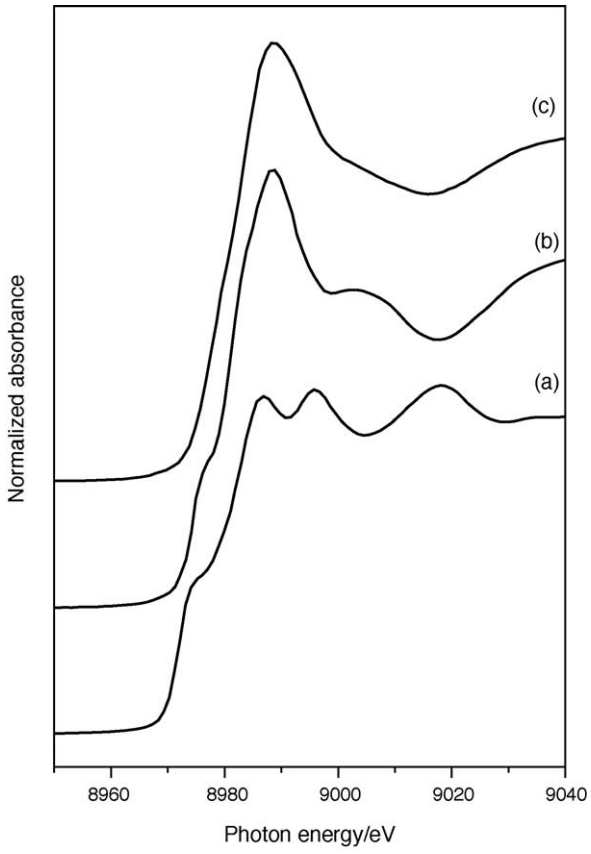

Fig. 4. Cu K-edge XANES spectra of reference compounds: (a) Cu foil; (b) CuO; and (c) $Cu(OH)_2$.

reduction of surface hydroxy groups led to the decrease of interaction between copper and zirconia. The copper species began to agglomeration. Thus, the CuO cluster formed on the support and dispersion decreased obviously. This was in conformity with the N_2O-titration and XRD results. However, for the Fe-$CuMnZrO_2$ catalysts, their XANES spectra showed similar to that for $Cu(OH)_2$ even calcined at 873 K (see Fig. 3B). This indicated that iron could enhance the stability of $Cu(OH)_2$ species by stabilizing the amorphous phase of zirconia at high temperature.

Fig. 5 showed the background subtracted k^3-weighted EXAFS oscillations, $k^3\chi$ (k), for $CuMnZrO_2$ and Fe-$CuMnZrO_2$ catalysts calcined at different temperature. For $CuMnZrO_2$ catalysts calcined at either 873 or 1073 K, fine structures characteristic of CuO all appeared at 8.0 and 8.5 $Å^{-1}$, while the same phenomenon appeared for Fe-$CuMnZrO_2$ catalyst calcined at 1073 K. This was in agreement with the XANES results in Fig. 3. The corresponding partial radial distribution functions (partial RDFs) obtained by Fourier transforms of $k^3\chi$ (k) were shown in Fig. 6 ($\Delta k = 3.0$–11.5 $Å^{-1}$). The Δk values were restricted to be relatively narrow, because the Hf L_3-edge (9561 eV) of HfO_2 (present as an impurity in the ZrO_2 used) severely hampered extraction of Cu K-edge oscillations at higher k values. The RDF, for $CuMnZrO_2$ catalysts calcined at both of 623 and 723 K, were significantly different from that of CuO or $Cu(OH)_2$ [29], suggesting formation of a copper species in a distinct local structure. On the other hand, the absence of Cu–Cu bonding suggested that the Cu^{2+} species were highly dispersed on the zirconia surface. However, for $CuMnZrO_2$ calcined over 873 K, a weak peak due to Cu–Cu bonding emerged at 2.8–2.9 Å (uncorrected for phase shifts), indicating the formation of CuO clusters. It was noteworthy that the presence of iron clearly favored remaining the highly copper dispersion. The Cu–Cu bonding only appeared on the Fe-$CuMnZrO_2$ catalyst calcined at 1073 K.

Structural parameters, as derived from an EXAFS analysis, were summarized in Table 2. In Cheah et al.'s research on the XAFS study of copper model compounds, they indicated that, due to the Jahn–Teller effect, the first coordination shell of Cu^{2+} was generally a distorted octahedron with four short bonds to equatorial ligands and two longer bonds to axial ligands [29]. However, the axial Cu–O bonds were difficult to characterize quantitatively by XAFS spectroscopy due to their very large Debye–Waller factors ($\Delta\sigma^2 > 0.02$ $Å^2$). Their distances also could not be determined accurately. As a result, the four equatorial O atoms were only found to comprise the main EXAFS oscillations in the spectra [29]. Herein, the Cu–O coordination numbers for the catalysts, which showed $Cu(OH)_2$ structure in an octahedral symmetry in XANES, were close or less than 4.0 as listed in Table 2. However, for the catalysts calcined at higher temperature, the Cu–O coordination numbers and distance was very close or equal to 4.0 and 1.95 Å, indicating the formation of CuO cluster which had a densely structure.

3.3. Temperature-programmed reduction

Fig. 7A presented the TPR profiles of $CuMnZrO_2$ catalysts. Two peaks of H_2 consumption were observed, corresponding to the reduction of highly dispersed copper species (at low temperature) and bulk CuO species (at high temperature), respectively [30]. Moreover, the area of the peak at low temperature monotonously decreased and synchronously shifted to higher temperature with the rise of calcination temperature. This illustrated that the copper species aggregated when the catalyst was calcined at high temperature. Apparently, the reduction behavior of $CuMnZrO_2$ catalyst calcined at 1073 K was quite different from that observed on the others, suggesting that new phases formed. It might be due to the formation of spinel compounds, $CuMn_2O_4$, as revealed in XRD (see Fig. 2), which hindered the reduction of copper species as envisaged in TPR profiles.

Compared with $CuMnZrO_2$ catalyst, the Fe-$CuMnZrO_2$ catalyst calcined at 623 K exhibited a higher intensity for the low temperature peak than that at high temperature (see Fig. 7B). It was worthy noted that when the calcination temperature increased from 623 to 873 K, the intensity of peak at 505 K decreased and shifted to lower temperature, while the intensity of peak at 530 K increased. The highly dispersed copper species were amorphous, which could be reduced

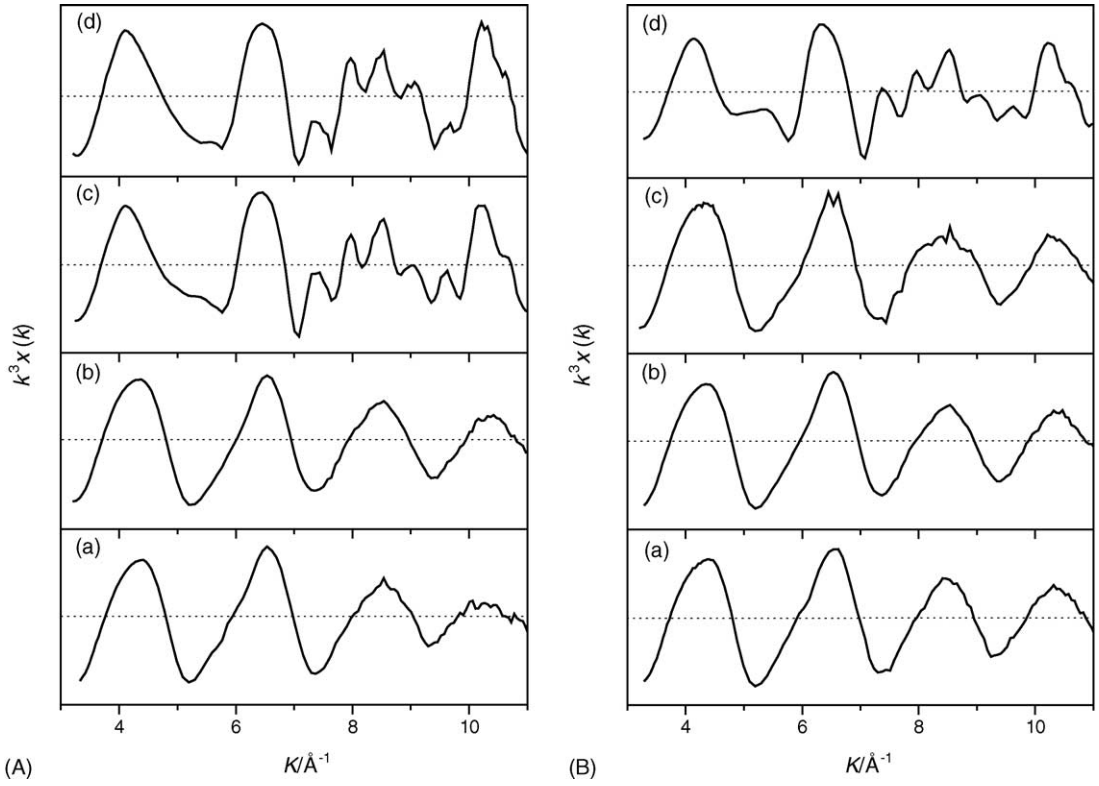

Fig. 5. k^3-weighted EXAFS oscillations for the $CuMnZrO_2$ (A) and Fe-$CuMnZrO_2$ (B) catalysts calcined at various temperatures: (a) 623 K; (b) 723 K; (c) 873 K; and (d) 1073 K.

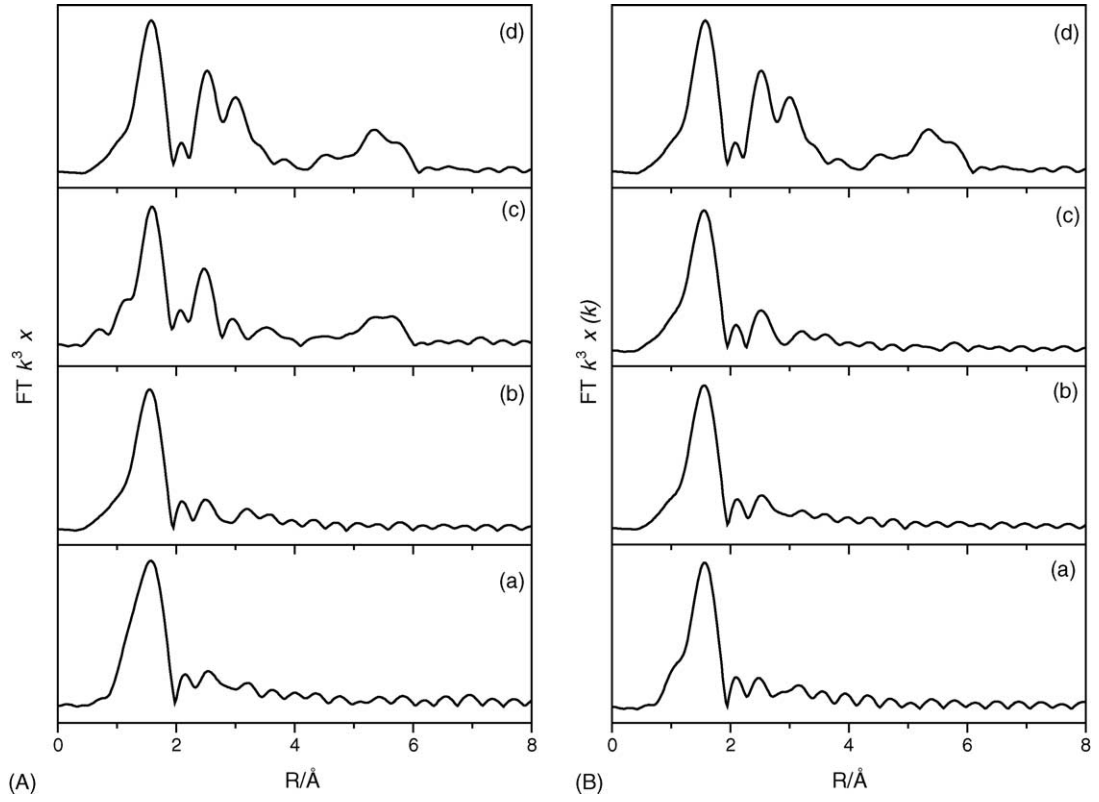

Fig. 6. Radial distribution functions obtained by Fourier transforming of EXAFS spectra of the $CuMnZrO_2$ (A) and Fe-$CuMnZrO_2$ (B) catalysts: (a) 623 K; (b) 723 K; (c) 873 K; and (d) 1073 K.

Table 2
Curve-fitting results of Cu—O in the $CuMnZrO_2$ and Fe-$CuMnZrO_2$ catalysts

Catalysts	Calcination temperature (K)	Shell	N	R (Å)	$\Delta\sigma^2$ (Å^2)	R factor (%)	Fitting range (Å^{-1})
$CuMnZrO_2$	623	Cu—O[a]	3.5	1.96	0.006	2.3	1.4–11.8
	723	Cu—O[a]	3.7	1.98	0.003	3.7	1.3–12.3
	873	Cu—O[a]	3.8	1.95	0.001	3.5	1.3–13.2
	1073	Cu—O[a]	4.0	1.94	0.0009	3.0	1.3–13.4
Fe-$CuMnZrO_2$	623	Cu—O[a]	3.5	1.97	0.005	4.9	1.3–12.3
	723	Cu—O[a]	3.4	1.98	0.005	4.5	1.2–12.3
	873	Cu—O[a]	3.6	1.96	0.004	3.2	1.5–11.3
	1073	Cu—O[a]	3.9	1.95	0.001	3.0	1.2–12.9

[a] Inverse-fourier range: $\Delta R = 1.0$–2.0 Å.

easily due to their loose structure and the strong interaction between copper species and zirconia [31]. The reduction of highly dispersed copper species shifted to low temperature, suggesting that the copper crystallite sizes became smaller [30]. On the other hand, such a result indicated that with the rise of calcination temperature, the interaction between copper and iron decreased because this interaction could increase the temperature of copper species reduction [32]. Notably, no obviously peak of H_2 consumption was found at higher temperature, suggesting that the iron was hardly reduced. It was possible that the interaction between iron and zirconia was too strong to reduce the hematite to Fe^0. Castro and coworkers reported that the formation of Fe^0 species could be hindered by the interaction of Fe^{2+} ions with the zirconia support [33]. However, metallic oxides particles shrank and crystallization when calcined at 1073 K, suggesting that the metal-support interface was destroyed and the interaction between metallic oxide and support decreased. The metal species migrated to surface and formed new phases. Moreover, the formation of spinel compounds ($CuMn_2O_4$, $CuFe_2O_4$) hindered the reduction of copper species as envisaged in TPR profiles because of the strong interaction between them.

3.4. Catalytic activity for carbon monoxide hydrogenation

$CuMnZrO_2$ catalyst showed the high activity and selectivity towards methanol synthesis. However, the activity decreased monotonously with the rise of calcination temperature as shown in Table 3. The selectivity for alcohols showed a maximum when the catalyst calcined at 873 K. The addition of iron suppressed the hydrogenation activity with the

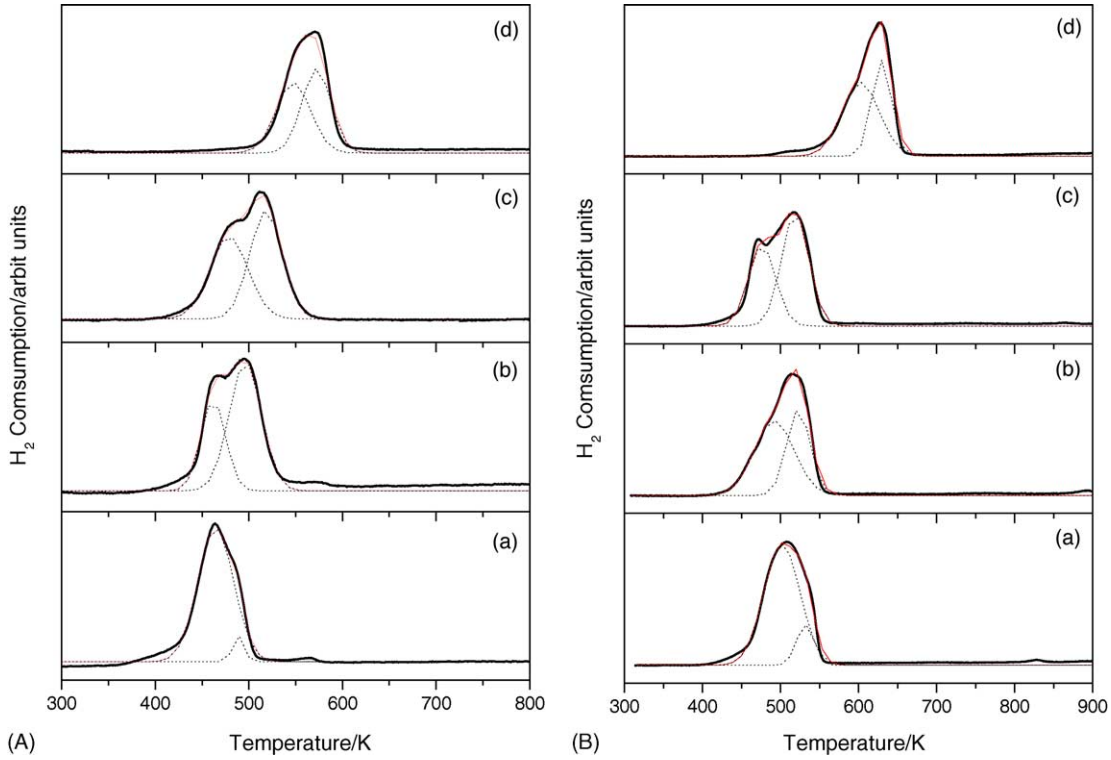

Fig. 7. H_2-TPR profiles of the $CuMnZrO_2$ (A) and Fe-$CuMnZrO_2$ (B) catalysts calcined at various temperatures: (a) 623 K; (b) 723 K; (c) 873 K; and (d) 1073 K.

Table 3
Effect of calcination temperature on the performances of catalysts for CO hydrogenation

Catalysts	Calcination temperature (K)	CO conversion (%)	Carbon selectivity[a] (%)			Alcohols yield ($g\,mL^{-1}\,h^{-1}$)	C_2^+ OH in alcohols (wt.%)	TOF[b]
			CO_2	HC	ROH			
$CuMnZrO_2$	623	37.3	18.0	17.9	64.1	0.85	6.0	5.9
	723	29.3	14. 6	13.8	71.6	0.77	3.8	6.7
	873	21.7	8.8	6.9	84.3	0.65	2.3	16.3
	1073	8.2	26.3	29.8	43.9	0.12	7.8	12.1
Fe-$CuMnZrO_2$	623	29.4	27.7	43.5	29.1	0.42	18.1	4.1
	723	12.6	15.0	26.1	58.9	0.30	8.4	1.8
	873	11.9	15.3	15.6	69.1	0.34	5.0	1.3
	1073	33.2	20.3	64.9	14.8	0.15	33.7	19.1

Reaction conditions: 573 K, 8.0 MPa, 8000 h^{-1}, $H_2/CO = 2.0$.
[a] Selectivity based on number of atoms per gram carbon = (number of CO converted to given product/total number of CO converted) × 100%.
[b] TOF: CO conversion rate on per copper surface (m^2).

improvement of higher alcohols synthesis. The carbon chain growth was noticeably observed with the proportion of C_2^+ alcohols more than 18% when the catalyst calcined at 623 K. Moreover, the selectivity for alcohols increased in line with the calcination temperatures increasing from 623 to 873 K, while the proportion of C_2^+ alcohols in the total alcohol fraction decreased.

On the $CuMnZrO_2$ catalyst, with the rise of calcination temperature the copper species agglomerated and the dispersion decreased that led to decrease of catalytic activity. However, the TOF showed a maximum on the catalyst calcined at 873 K, suggesting that the interaction between copper species and support reached the peak. This interaction was considered as the important factor for methanol synthesis by several researches [34,35].

Compared with $CuMnZrO_2$, the addition of iron to the catalyst resulted in the suppression of overall catalytic activity, while it favored the higher alcohols synthesis. Courty et al. [10] investigated the Co modified Cu-Zn/Al_2O_3 catalyst, suggesting that suppression of the hydrogenation activity of Co would allow partially hydrogenated CH_x species to remain for longer periods, and these were involved in the C–C chain formation leading to the production of higher hydrocarbons and alcohols. On the basis of the XRD and XAFS results, iron enhanced the stability of the catalysts by stabilizing the amorphous phase of zirconia, and then the dispersion of copper species increased. However, the increase of copper dispersion did not improve the activity and the TOF reduced to minimum on the catalyst calcined at 873 K. This indicated that the iron–zirconia interaction suppressed the interaction between copper species and zirconia. On the other hand, the interaction between iron and zirconia hindered the reduction of iron oxide, and then copper–iron interaction weakened, which reduced the active sites for higher alcohol formation. As a result, the catalytic activity for higher alcohols synthesis reduced. When the Fe-$CuMnZrO_2$ catalyst calcined at 1073 K, it was found that the active phase greatly aggregated in XRD study. However, the overall activity increased consumingly. A large amount of hydrocarbons produced. At the same time, the proportion of higher alcohols in the liquid products was quite high. This might be explained by the enhanced interaction between copper and iron by formation of spinel compounds ($CuFe_2O_4$). It was reported that the copper–iron based catalyst had a high activity for carbon monoxide hydrogenation, such as Fischer–Tropsch synthesis [32].

4. Conclusion

The effect of iron promoter on the structure and catalytic performance of $CuMnZrO_2$ catalysts was investigated by comparison of iron-promoted and un-promoted catalysts calcined at different temperature. It was found that the change of metal-support interaction strongly influenced the surface and crystal structure of the catalyst and hence its catalytic performance. Low calcination temperature yielded poorly crystallized catalysts and favored the formation of a $Cu(OH)_2$-like structure. For the $CuMnZrO_2$ catalyst, with the rise of calcination temperature, surface area and dispersion of copper decreased, and the crystallization of zirconia occurred. Nevertheless, the copper–zirconia interaction increased in a way. The TOF showed a maximum on the catalyst calcined at 873 K. The presence of iron could suppress agglomeration of copper species and crystallization of amorphous zirconia. The dispersion of copper was enhanced on the Fe-$CuMnZrO_2$ catalyst. However, the addition of iron to the catalyst resulted in the suppression of overall catalytic activity. On the one hand, the increase of iron–zirconia interaction with the rise of calcination temperature suppressed the interaction between copper species and zirconia. On the other hand, the interaction between iron and zirconia hindered the reduction of iron oxide, and then copper–iron interaction weakened, which reduced the active sites for higher alcohol formation.

Acknowledgments

This work was supported by the State Key Foundation Project for Development and Research of China

(G1999022400) and Knowledge Innovation Program of Chinese Academy of Sciences (KGCX2-302).

References

[1] J.P. Hidermann, G.J. Hutchings, A. Kiennemann, Catal. Rev. Sci. Eng. 35 (1993) 1.
[2] X.D. Xu, E.B.M. Doesberg, J.J.F. Scholten, Catal. Today 2 (1987) 125.
[3] R.G. Herman, Catal. Today 55 (2000) 233.
[4] A.B. Stiles, F. Chen, J.B. Harrison, X. Hu, D.A. Storm, H.X. Yang, Ind. Eng. Chem. Res. 30 (1991) 811.
[5] A. Kiennemann, C. Diagne, J.P. Hindermann, P. Chaumette, P. Courty, Appl. Catal. 53 (1989) 197.
[6] W.M.H. Sachtler, Proceedings of the Eighth International Congress on Catalysis, vol. 1, Berlin, Verlag Chemie, Weinheim, 1984, p. 152.
[7] I. Boz, Catal. Lett. 87 (2003) 187.
[8] A. Calafat, J. Laine, J. Catal. 147 (1994) 88.
[9] W. Chu, R. Kieffer, A. Kiennemann, J.P. Hindermann, Appl. Catal. A: Gen. 121 (1995) 95.
[10] P. Courty, D. Durand, E. Freund, A. Sugier, J. Mol. Catal. 17 (1982) 241.
[11] R.M. Bailliard-Letournel, A.J. Gomez Cobo, C. Mirodatos, M. Primet, J.A. Dalmon, Catal. Lett. 2 (1989) 149.
[12] J.E. Baker, R. Burch, Y. Niu, Appl. Catal. 73 (1991) 135.
[13] G.R. Sheffer, T.S. King, Appl. Catal. 44 (1988) 153.
[14] N. Zhao, R. Xu, W. Wei, Y. Sun, React. Kinet. Catal. Lett. 75 (2002) 297.
[15] R. Xu, Z. Ma, C. Yang, W. Wei, W. Li, Y. Sun, J. Mol. Catal. A 218 (2004) 133.
[16] J.W. Evans, M.S. Wainwright, A.J. Bridgewater, D.J. Youny, Appl. Catal. 7 (1983) 75.
[17] T. Huang, T. Yu, S. Chang, Appl. Catal. 52 (1989) 157.
[18] H. Aritani, N. Akasaka, T. Tanaka, T. Funabiki, S. Yoshida, H. Gotoh, Y. Okamoto, J. Chem. Soc., Faraday Trans. 92 (1996) 2625.
[19] H. Aritani, T. Tanaka, N. Akasaka, S. Yoshida, H. Gotoh, Y. Okamoto, J. Catal. 168 (1997) 412.
[20] B.S. Clausen, B. Lengeler, B.S. Rasmussen, J. Phys. Chem. 89 (1985) 2319.
[21] K. Tohji, Y. Udagawa, T. Mizushima, A. Ueno, J. Phys. Chem. 89 (1985) 5671.
[22] M.S. Tzou, M. Kusunoki, K. Asakura, H. Kuroda, G. Moretti, W.H.M. Sachtler, J. Phys. Chem. 95 (1991) 5210.
[23] L.S. Kau, D.J. Spira-Solomon, J.E. Penner-Hahn, K.O. Hodgson, E.I. Solomon, J. Am. Chem. Soc. 109 (1987) 6433.
[24] B. Hedman, K.O. Hodgson, E.I. Solomon, J. Am. Chem. Soc. 112 (1990) 1643.
[25] S.-F. Cheah, G.E. Brown Jr., G.A. Parks, J. Colloid Interface Sci. 208 (1998) 110.
[26] P.W. Schindler, B. Furst, R. Dick, P.U. Wolf, J. Colloid Interface Sci. 55 (1976) 469.
[27] Y. Okamoto, H. Gotoh, H. Aritani, T. Tanaka, S. Yoshida, J. Chem. Soc. Faraday Trans. 93 (1997) 3879.
[28] B. Bachiller-Baeza, I. Rodriguez-Ramos, A. Guerrero-Ruiz, Langmuir 14 (1998) 3556.
[29] S.-F. Cheah, G.E. Brown Jr., G.A. Parks, Am. Mineral. 85 (2000) 118.
[30] M. Shimokawabe, H. Asakawa, N. Takezawa, Appl. Catal. 59 (1990) 45.
[31] R. Zhou, T. Yu, X. Jiang, F. Chen, X. Zheng, Appl. Surf. Sci. 148 (1999) 263.
[32] D.B. Bukur, D. Mukesk, S.A. Patel, Ind. Eng. Chem. Res. 29 (1990) 194.
[33] L. Castro, P. Reyes, C.M. De Correa, J. Sol–Gel Sci. Technol. 25 (2002) 159.
[34] D. Bianchi, J. Gass, M. Khalfallah, S. Teichner, Appl. Catal. A: Gen. 101 (1993) 297.
[35] I.A. Fisher, A.T. Bell, J. Catal. 178 (1998) 153.